

Characteristic Analysis for 2D Steady Supersonic Reacting Flow: Effect of Confinement on Detonation Flows

Mark Short and Carlos Chiquete
Los Alamos National Laboratory
Los Alamos, New Mexico, USA

1 Introduction

Steady detonation propagation in multi-dimensional high explosive (HE) geometries is determined by the energy release that occurs within a structure called the detonation driving zone (DDZ). This is the subsonic flow region bounded by the detonation shock and sonic flow locus (in a frame traveling with the steadily propagating detonation front). The properties of the material surrounding the HE have a significant influence on the structure on the DDZ [1]. For low impedance confiners, the confinement is denoted as weak, and typically a Prandtl-Meyer (PM) fan extending into the supersonic flow regime sits at the intersection of the detonation shock, sonic flow locus and HE/confiner material boundary [1]. Weak confinement materials were previously thought not to influence the DDZ structure. For higher impedance confiners, the sonic locus drops downstream of the detonation shock at the HE/confiner boundary, and the presence of the confinement is communicated directly to the DDZ through the material interface. In recent work by Chiquete and Short [2], it was shown that the influence of the confinement on the DDZ structure is significantly more complicated. Specifically, information can travel from the PM fan for weak confinement and from the material interface boundaries downstream of the sonic locus for strong confinement, through the supersonic flow region downstream of the sonic locus, and impact on the sonic locus. Consequently, information about the confinement is deposited into the DDZ. Chiquete and Short [2] employed a modeling assumption whereby the shape of material boundary streamline was imposed on the flow solution to mimic the effect of weak or strong confinement.

In the current study, we examine the influence of information propagation through the supersonic flow regime for the case of weak confinement using a full multi-material simulation approach. We first derive the flow characteristics for 2D steady, reactive, rotational, and non-isentropic flow in both a 2D planar slab geometry and 2D circular arc geometry. We then consider three aspects of the weak confinement problem. These examine whether a curved material boundary interface, as opposed to the linear shape assumed in [2], changes the nature of information flow through the supersonic region. Second, we study the influence that a newly discovered PM expansion wave that emerges at the sonic flow point on the centerline of a 2D planar slab geometry has on the shape of the DDZ. Third, we study the effect of geometry on characteristic information flow through the supersonic regime that impacts on the DDZ, contrasting the behavior between 2D planar slab and 2D circular arc geometries.

2 Model

We consider a detonation propagating steadily in a 2D planar slab or circular arc geometry (Fig. 1), with the HE surrounded by a low-impedance elastomer [1, 3]. For the high pressures induced by detonation loading, we can model the flow in both the explosive and confiner with the compressible Euler equations,

$$\frac{D\rho}{Dt} + \rho \nabla \cdot \mathbf{u} = 0, \quad \frac{D\mathbf{u}}{Dt} = -\frac{1}{\rho} \nabla p, \quad \frac{De}{Dt} = \frac{p}{\rho^2} \frac{D\rho}{Dt}, \quad (1)$$

for density ρ , pressure p , particle velocity $\mathbf{u} = (u, v)$ and specific internal energy e . The material derivative $D/Dt = \partial/\partial t + \mathbf{u} \cdot \nabla$, where t is time. The flow evolution in the reactive and inert confinement layers is determined by the specification of e for each material.

For the HE, we use a stiffened-gas condensed-phase detonation model [1, 3], whereupon the equation of state (EOS) model for the internal energy, e , the specific reaction enthalpy of the HE, q , and the frozen sound speed, c , are given by

$$e = \frac{p + A}{(\gamma - 1)\rho} - q\lambda, \quad q = \frac{D_{CJ}^2}{2(\gamma^2 - 1)} \left(1 - \frac{A}{\rho_0 D_{CJ}^2}\right)^2, \quad c = \left[\frac{\gamma p + A}{\rho}\right]^{1/2}, \quad (2)$$

respectively, where γ is the adiabatic exponent, A is the stiffened gas constant, ρ_0 is the initial density of the HE and D_{CJ} is the Chapman-Jouguet (CJ) speed. Also, λ is the reaction progress variable ($0 \leq \lambda \leq 1$). The associated reaction model is

$$\frac{D\lambda}{Dt} = \Lambda = kp^n(1 - \lambda)^\nu, \quad (3)$$

where k is a rate constant, n is the pressure exponent and ν is a reaction order variable. Reference scales are given in [3], where the reference length scale is the length behind the shock in the steady, planar Chapman-Jouguet detonation wave at which half of the reactant has been consumed. Relations to physical length scales for a variety of HEs are discussed in [1]. We take

$$\rho_0 = 2, \quad A = 12.8, \quad D_{CJ} = 8, \quad \gamma = 3, \quad n = 1, \quad \nu = 1/2, \quad (4)$$

as for previous studies [1, 3], for which $q = 3.24$ and $k \approx 0.051359$.

For the elastomer (El) confiner layer region, again as in previous studies e.g. [1, 3], we use a Mie-Grüneisen EOS with a reference curve that is based on a linear shock speed (U_s) - particle speed (u_p) Hugoniot-state variation, where $U_s = c_c + su_p$. Here c_c is the sound speed at the ambient state, while s is the slope dU_s/du_p . The corresponding internal energy of the Mie-Grüneisen EOS is

$$e = \frac{c_c^2 \sigma^2}{2(1 - s\sigma)^2} + \frac{1}{\Gamma_{c0} \rho_{c0}} \left(p - \frac{\rho_{c0} c_c^2 \sigma}{(1 - s\sigma)^2} \right), \quad \sigma = 1 - \frac{\rho_{c0}}{\rho}, \quad (5)$$

where Γ_{c0} is the Grüneisen gamma and ρ_{c0} is the ambient confiner density, where $c_c = 1.127$, $s = 1.2$, $\rho_{c0} = 0.84$, and $\Gamma_{c0} = 1.5$. The El layer provides no confinement effect on the detonation propagation mechanism in the historical sense defined in [1].

For the slab problem, a detonation propagates axially in an HE layer, with El bounding the HE (Fig. 1[L]). Computationally, symmetry conditions are applied along the bottom boundary of Fig. 1[L] ($y = 0$), so that for a total HE height W_{HE} , the HE region shown has height $W_{HE}/2$. The elastomer layer thickness is W_{El} and the channel length is L , so that the computational domain is rectangular with the lower left and upper right corners located at $(0, 0)$ and $(L, W_{HE}/2 + W_{El})$, respectively. Outflow conditions are applied along the left, right and top boundaries. Here, $L = 450$ in all cases, while $W_{El} = 30$, wide

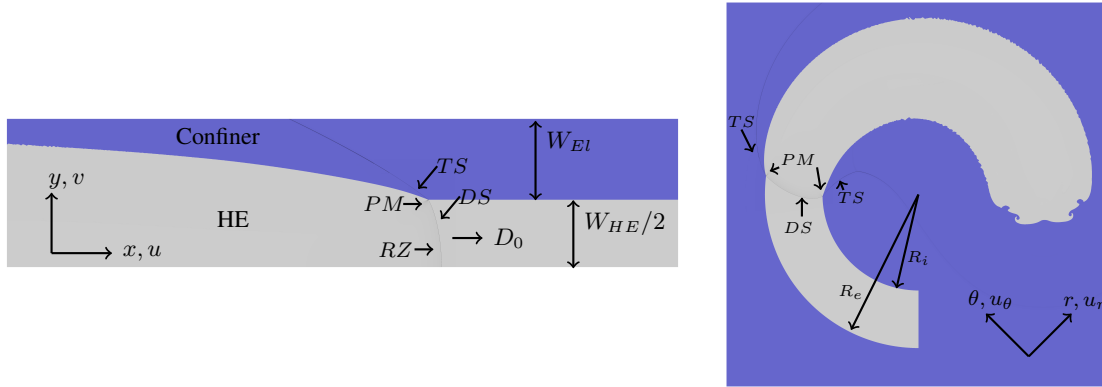


Figure 1: [L] A section of the 2D planar slab computational geometry showing HE (light grey) and confiner (blue) regions. Also shown is a steady stage of detonation propagation with $W_{HE} = 50$ and $W_{El} = 30$. The dark lines represent a weighted pressure gradient image representation of the primary flow structures [3], showing the detonation shock (DS), reaction zone (RZ), reflected PM waves at the HE-detonation/confiner interface (PM) and transmitted shock in the confiner (TS). [R] As for [L], but for the circular arc geometry with $R_i = 100$, $R_e = 160$ and $R_D = 200$.

enough for the upper boundary to have no influence on the DDZ region or flowing flow in the vicinity of the DDZ region, as determined from a characteristic analysis. The steady axial detonation speed is D_0 . For the arc problem, the HE region extends from $0 \leq \theta \leq 3\pi/2$ in polar coordinates (r, θ) , as shown in Fig. 1[R]. The inner radius of the HE arc is R_i , while its outer radius is R_e . The HE arc is surrounded everywhere on the inner and outer surfaces by the El. The total computational region is a square box with sides of length $2R_D$, $R_D > R_e$, having corners located at $(-R_D, -R_D)$, $(-R_D, R_D)$, (R_D, R_D) and $(R_D, -R_D)$ in Cartesian coordinates. The outer edges of the computational area have an outflow condition applied. Here, $R_D = 200$. The angular speed of the steadily rotating detonation is denoted by ω_0 .

The flow equations in the HE and El regions are integrated with a cell-centered finite volume method on a Cartesian mesh within the multi-material simulation framework AMRITA-MultiMat [3]. A second-order minmod spatial reconstruction with a Lax-Friedrichs flux is used together with a second-order total variation diminishing Runge-Kutta time integration. Material interfaces are treated with a Ghost Fluid method, where, for the computations below, we construct a local linearized Riemann solution based on the real fluid state on either side of the interface to populate the relevant ghost fluid states for each real material. The interface is evolved using a level set strategy. A block structured adaptive-mesh-refinement capability is also employed [3]. Two levels of refinement are used with a refinement factor of 4 for each level. The resolution of the finest grid was 320 points per the unit (half-reaction zone) length defined above.

3 Characteristic Analysis

For the 2D planar slab geometry, with the detonation propagating axially with speed D_0 , the Euler equations with $\mathbf{w} = (\rho, u, v, p, \lambda)^T$ can be written in the steady traveling frame as

$$\mathbf{w}_{\bar{x}} + \mathbf{A}\mathbf{w}_{\bar{y}} = \mathbf{a} \quad (6)$$

where \mathbf{A} and \mathbf{a} are given by

$$\begin{pmatrix} \frac{v}{u-D_0} & \frac{\rho v}{c^2-(u-D_0)^2} & -\frac{\rho(u-D_0)}{c^2-(u-D_0)^2} & -\frac{v}{(u-D_0)(c^2-(u-D_0)^2)} & 0 \\ 0 & -\frac{(u-D_0)v}{c^2-(u-D_0)^2} & \frac{c^2}{c^2-(u-D_0)^2} & \frac{v}{\rho(c^2-(u-D_0)^2)} & 0 \\ 0 & 0 & \frac{v}{u-D_0} & \frac{\rho(u-D_0)}{\rho(c^2-(u-D_0)^2)} & 0 \\ 0 & \frac{\rho c^2 v}{c^2-(u-D_0)^2} & -\frac{\rho c^2(u-D_0)}{c^2-(u-D_0)^2} & -\frac{(u-D_0)v}{c^2-(u-D_0)^2} & 0 \\ 0 & 0 & 0 & 0 & \frac{v}{u-D_0} \end{pmatrix}, \begin{pmatrix} \frac{e,\lambda\Lambda}{e,p(u-D_0)(c^2-(u-D_0)^2)} \\ -\frac{e,\lambda\Lambda}{e,p\rho(c^2-(u-D_0)^2)} \\ 0 \\ \frac{e,\lambda\Lambda(u-D_0)}{e,p(c^2-(u-D_0)^2)} \\ \frac{\Lambda}{u-D_0} \end{pmatrix}, \quad (7)$$

respectively. The five eigenvalues of \mathbf{A} ($\alpha_1 \dots \alpha_5$) lead to the characteristic path constructions

$$\frac{d\bar{y}}{d\bar{x}} = \alpha_{1,2,3} = \frac{v}{u-D_0}, \quad \frac{d\bar{y}}{d\bar{x}} = \alpha_{4,5} = \frac{(u-D_0)v \pm c\sqrt{(u-D_0)^2 + v^2 - c^2}}{(u-D_0)^2 - c^2}, \quad (8)$$

with the first set $\alpha_{1,2,3}$ corresponding to C^0 flow streamlines in the steady frame, and the second set to wave signal propagation. The $+$ sign in the numerator of (8) (α_4) is associated with C^+ characteristics that propagate information from right to left with reference to Fig. 2 and 3, while the $-$ sign in (8) (α_5) is associated with C^- characteristics propagating information from left to right. On the sonic locus $\sqrt{(u-D_0)^2 + v^2} = c$, and thus $d\bar{y}/d\bar{x}$ is the same for both the C^+ and C^- characteristics, so that both characteristic families enter or leave the sonic locus with the same slope. On the symmetry line at the sonic locus, $d\bar{x}/d\bar{y} = 0$ for both C^+ and C^- characteristics. The streamlines C^0 are also normal to the C^+ and C^- characteristics along the sonic line. Calculating the left eigenvectors of \mathbf{A} (the transpose of the right eigenvectors of \mathbf{A}^T) corresponding to $\alpha_1 \dots \alpha_5$, and then multiplying (6) by each left eigenvector separately, leads to the characteristic equations

$$\begin{aligned} -c^2\rho_{\bar{x}} + p_{\bar{x}} + \frac{v}{(u-D_0)} [-c^2\rho_{\bar{y}} + p_{\bar{y}}] &= -\frac{e,\lambda\Lambda}{e,p(u-D_0)}, \quad \lambda_{,\bar{x}} + \frac{v}{(u-D_0)}\lambda_{,\bar{y}} = \frac{\Lambda}{(u-D_0)}, \\ \frac{p_{,\bar{x}}}{\rho} + (u-D_0)u_{,\bar{x}} + vv_{,\bar{x}} + \frac{v}{(u-D_0)} \left[\frac{p_{,\bar{y}}}{\rho} + (u-D_0)u_{,\bar{y}} + vv_{,\bar{y}} \right] &= 0, \\ vu_{\bar{x}} - (u-D_0)v_{,\bar{x}} \mp \frac{p_{,\bar{x}}}{\rho c}U + \alpha_{4,5} \left[vu_{\bar{y}} - (u-D_0)v_{,\bar{y}} \mp \frac{p_{,\bar{y}}}{\rho c}U \right] &= \\ \frac{e,\lambda\Lambda}{\rho ce,p(c^2-(u-D_0)^2)} [-cv \mp (u-D_0)U], & \end{aligned} \quad (9)$$

where $U = \sqrt{(u-D_0)^2 + v^2 - c^2}$. A Bernoulli integral and expression for the evolution of entropy along a streamline in the presence of reaction may also be derived. We can repeat the above analysis for the 2D circular arc geometry relative to a frame rotating with the detonation shock front (angular speed ω_0), along which each location on the shock moves with speed $(-r\omega_0 \sin \theta, r\omega_0 \cos \theta)$ in a Cartesian frame. With the flow velocity vector in polar coordinates (u_r, u_θ) , this leads to the characteristic paths

$$\frac{d\bar{\theta}}{d\bar{r}} = \alpha_{1,2,3} = \frac{u_\theta - r\omega_0}{ru_r}, \quad \frac{d\bar{\theta}}{d\bar{r}} = \alpha_{4,5} = \frac{u_r(u_\theta - r\omega_0) \pm c\sqrt{u_r^2 + (u_\theta - r\omega_0)^2 - c^2}}{r(u_r^2 - c^2)}. \quad (10)$$

The sonic locus is determined by the set of points for which $[u_r^2 + (u_\theta - r\omega_0)^2]^{1/2} = c$.

4 Slab and Arc Geometry Analysis

For the 2D planar slab configuration, we refer to an idealized reference case consisting of a spatially structureless CJ detonation which is flat, and a material confinement boundary deflection which is linear and starts at the CJ detonation/material interface intersection point. A Prandtl-Meyer (PM) fan lies

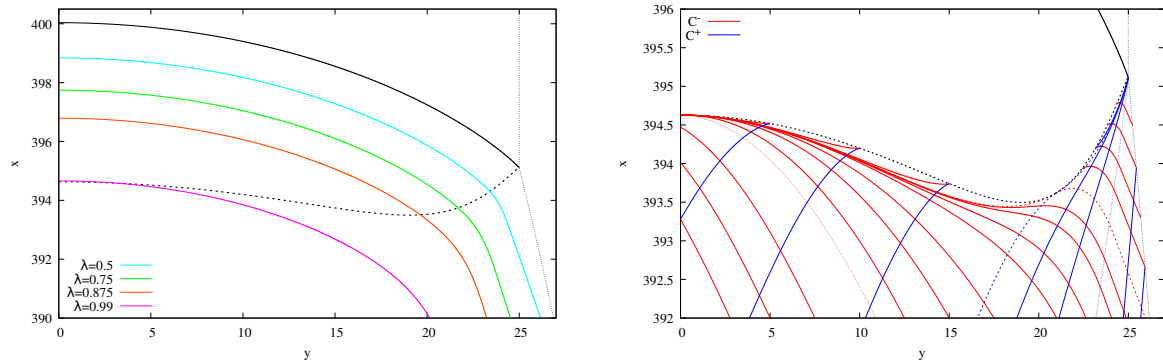


Figure 2: [L] The structure of the subsonic DDZ region propagating axially in the slab configuration with $W_{HE} = 50$. The black solid line is the detonation shock, the black dashed line is the sonic locus and the black dotted line is the HE/confiner material interface. A set of reaction contours are also shown. [R] The C^+ and C^- characteristic paths in the supersonic flow region. Here $D_0 = 7.198$.

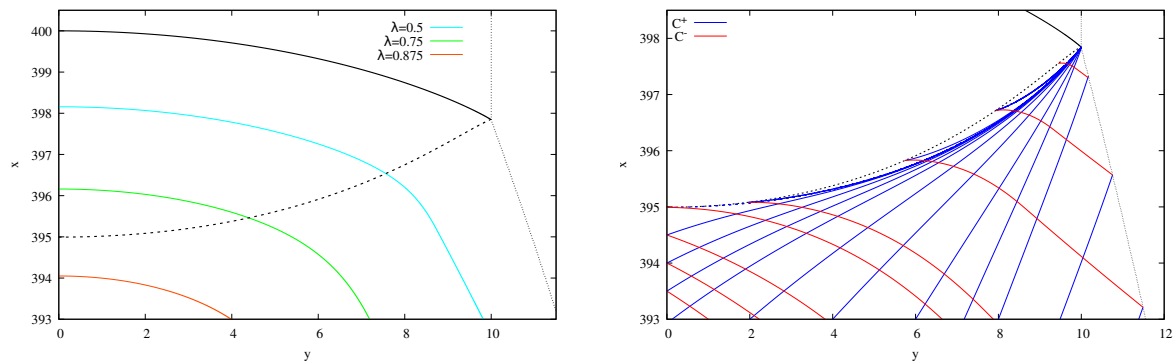


Figure 3: As for Fig. 2, but with $W_{HE} = 20$. Here $D_0 = 5.781$.

between the deflected material interface and the CJ plane, which the leading C^+ PM fan characteristic coincident with the CJ plane. Similarly, the leading C^- characteristic lies in the CJ wave sonic plane.

When the reaction zone has a spatial structure due to a finite rate of reaction, the flow field is significantly more complex. Figure 2[L] shows the steady 2D DDZ structure for $W_{HE} = 50$, bounded by the detonation shock and sonic flow locus. The shock and sonic locus intersect at the HE/EI material interface. Reaction progress contours show weakened reaction at the HE charge edge. The sonic locus is divergently curved near the charge symmetry line, but becomes convergent near the charge edge. A PM fan with an origin at the detonation shock/material interface intersection point lies between the sonic surface and material interface. Prior to the work of Chiquete and Short [2], it had been believed the PM fan had no influence on the DDZ structure. Figure 2[R] shows the corresponding set of C^+ and C^- characteristic paths in the supersonic flow region downstream of the sonic locus. The C^+ PM fan at the shock/sonic locus/material interface intersection point is clearly observed. Some of its C^+ characteristics bend toward and intersect the sonic surface and deposit information about the fan on the sonic locus of the DDZ. This complex behavior arises due to the effects of reaction beyond the sonic locus [2]. The limiting C^+ characteristic, shown as a blue dashed line, defines the region that the C^+ PM fan impacts on the DDZ sonic locus, and is tangent to the sonic locus at its intersection point. The bulk of the sonic line, however, is influenced by a PM fan whose origin is at the sonic locus along the axial symmetry line. C^- lines leave the origin and turn back into the sonic locus, depositing information about the symmetry line fan on the sonic locus and affecting the DDZ structure (Fig. 2[R]). Evidently, this symmetry line PM fan behavior helps pull the sonic locus downstream, generating the complex DDZ sonic locus shape seen in Fig. 2. Note that the region of influence of this PM fan (defined by the dotted C^- characteristic,

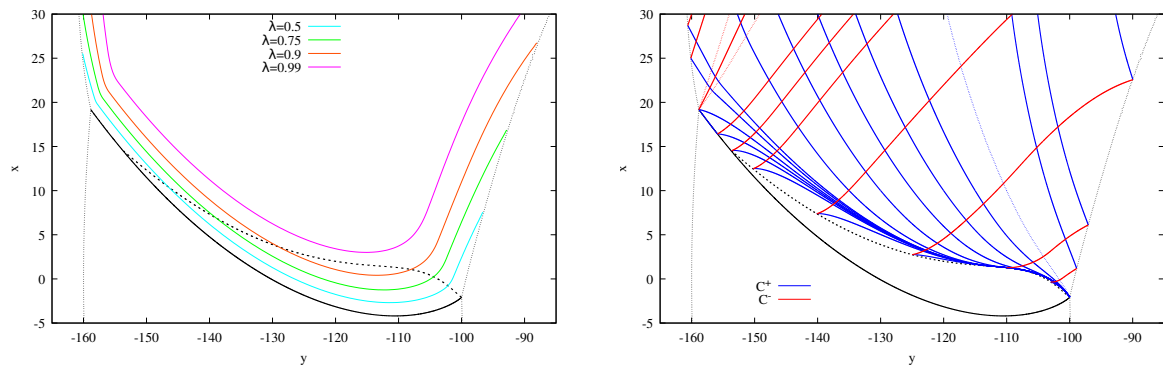


Figure 4: [L] The structure of the subsonic DDZ region sweeping around the 100 (R_i) x 160 (R_e) 2D circular arc configuration. [R] The C^+ and C^- characteristic paths in the supersonic flow region. Both plots are shown in Cartesian coordinates. Here, the linear detonation speed on $r = R_i$ is $R_i\omega_0 = 5.727$.

the sonic line and the C^- limiting characteristic) is substantial downstream of the sonic plane.

As the charge size decreases, the sonic line loses its complex structure. Figure 3 shows the DDZ structure and C^+ and C^- characteristic paths for $W_{HE} = 20$. The sonic locus is entirely convergent, while the PM fan at the symmetry line has now disappeared. The C^+ characteristics from the PM fan at the material interface now intersect each point on the sonic locus, so that the sonic locus is entirely influenced by the PM confinement boundary fan. C^- characteristics move information off the sonic locus and into the material interface downstream of the sonic locus/material interface point. We observe that in both cases, the curved material interface does not significantly alter the mechanics of characteristic path information propagation seen in the idealized case studied in [2].

The DDZ structure and boundary influence for weak confinement in a 2D circular arc configuration is even more complex. It was shown by Short et al. [3] that for thin enough arcs, the DDZ extends from the inner to outer arc surfaces. At a certain critical thickness, however, the sonic layer detaches from the outer surface at the same arc thickness that the detonation angular speed ω_0 limits to a constant, i.e., the outer arc boundary no longer appears to influence the DDZ. The DDZ structure for such a case is shown in Fig. 4[L] for $R_i = 100$ and $R_e = 160$. However, with the possibility that C^+ and C^- characteristics in the supersonic flow region can impact and deposit information on the DDZ, we need to fully understand why the outer surface no longer influences the DDZ. The corresponding C^+ and C^- characteristic paths (from (10)) are shown in Fig. 4[R]. The influence of the PM fan at the inner surface is substantial. A narrow band of C^+ fan characteristics leave the PM fan origin and intersect the complete DDZ sonic surface, depositing information on the sonic locus. Moreover, the influence of this C^+ fan covers a wide region downstream of the sonic surface as shown in Fig. 4[R]. On the other hand, the C^- characteristics all leave the sonic surface. There is a narrow band of C^- characteristics forming a PM fan at the outer surface, but none of the associated C^- characteristics intersect the sonic surface. This explains why the DDZ, and thus ω_0 , is unaffected by the outer surface. In summary, we have obtained significant insights on the influence of weak confinement on the HE DDZ structure for both the slab and arc geometries through a characteristic analysis for 2D, steady, non-isentropic flow.

References

- [1] M. Short and J.J. Quirk. High explosive detonation-confiner interactions. *Annu. Rev. Fluid Mech.*, 50:215–242, 2018.
- [2] C. Chiquete and M. Short. Characteristic path analysis of confinement influence on steady two-dimensional detonation propagation. *J. Fluid Mech.*, 863:789–816, 2019.
- [3] M. Short, J.J. Quirk, C.D. Chiquete, and C.D. Meyer. Detonation propagation in a circular arc: Reactive burn modelling. *J. Fluid Mech.*, 835:970–998, 2018.